

## REVIEW



CrossMark  
click for updates

Cite this: *J. Mater. Chem. B*, 2017, 5, 2714

## Electron microscopy for inorganic-type drug delivery nanocarriers for antitumoral applications: what does it reveal?

A. Baeza,<sup>a</sup> R. R. Castillo,<sup>a</sup> A. Torres-Pardo,<sup>b</sup> J. M. González-Calbet<sup>b</sup> and M. Vallet-Regí<sup>\*a</sup>

The use of nanoparticles with the ability to transport drugs in a selective and controllable manner directly to diseased tissues and cells has improved the therapeutic arsenal for addressing unmet clinical situations. In recent years, a vast number of nanocarriers with inorganic, organic, hybrid and even biological nature have been developed especially for their application in the oncology field. The exponential growth in the field of nanomedicine would not have been possible without the also-rapid expansion of electron microscopy techniques, which allow a more precise observation of nanometric objects. The use of these techniques provides a better understanding of the key parameters which rule the nanoparticles' synthesis and behavior. In this review, the recent advances made in the application of inorganic nanoparticles to clinical uses and the role which electron microscopy has played are presented.

Received 24th November 2016,  
Accepted 17th February 2017

DOI: 10.1039/c6tb03062a

rsc.li/materials-b

## Introduction

Inspired by the visionary speech of Richard Feynman in 1959 at the annual meeting of the American Physical Society, scientists with different backgrounds have struggled to understand the principles of the behaviour of matter in nanometer scale. Thanks to their efforts, nanotechnology is nowadays a well-established science and has significantly contributed to the development of diverse fields such as materials science, physics, chemistry and medicine, among others. Nanoparticles are currently at the root of a variety of application domains, spanning from catalysis and nanoelectronics to biomedicine or healthcare. In all cases, their functionality is tightly related to the ultimate structural and compositional details, as well as to their interactions with other particles in multicomponent-type materials. The progress of this science would not have been possible without the parallel development of electron microscopy, which has given the scientific community the opportunity to directly visualize the nanometer world. The broad range of electron microscopy techniques (imaging techniques, analytical spectroscopies, tomography, gas or liquid *in situ* experiments. . .) currently provide the means to reveal at the finest spatial scale, down to sub-Angstrom, the

2D and 3D information required to monitor the structure and functionalization of such nanometric systems as well as to rationalize their behaviour. In the last decades, the use of nanoparticles in medicine has provided new weapons to fight unmet diseases<sup>1</sup> and also helped in the development of more accurate diagnosis tools.<sup>2</sup> Their nanometric size allows a close interaction with their biological targets such as cells, bacteria or viruses, resulting in an improved therapeutic response with reduced side effects.<sup>3</sup> Simply encapsulating a drug within a nanoparticle produces several interesting advantages in comparison with the free drug, such as enhanced circulation time, higher drug concentration in the target zone, and the possibility of employing lipophilic drugs, which is the case for many anti-tumoral compounds.<sup>4</sup> The external surface of these carriers can be decorated with synthetic or natural biomolecules in order to detect the desired target, either a diseased tissue<sup>5</sup> or cell,<sup>6</sup> thus enhancing the selectivity of the nanocarrier. Additionally, these nanodevices can be engineered with stimuli-responsive properties in order to release their payloads only in the presence of certain stimuli, which further reduces the toxic side effects of the therapy. These stimuli could be specific to the treated disease, such as pH alterations and the presence of enzymes or molecules, or they can be externally applied, such as light, magnetic fields or ultrasound, among others.<sup>7</sup> For the development of these smart materials, recent advances in electron microscopy<sup>8,9</sup> have played an essential role allowing the precise visualization of both the particle morphology itself and its cargo and external functionalization. Due to the vast number of nanodevices reported, in this review, a brief description of the recent advances carried out in the

<sup>a</sup> Dpto. Química Inorgánica y Bioinorgánica, Facultad de Farmacia, Universidad Complutense de Madrid, Plaza Ramon y Cajal s/n, Instituto de Investigación Sanitaria Hospital 12 de Octubre i + 12, Centro de Investigación Biomédica en Red de Bioingeniería, Biomateriales y Nanomedicina (CIBER-BBN), Madrid, Spain. E-mail: vallet@ucm.es

<sup>b</sup> Dpto. de Química Inorgánica Facultad de Químicas, Universidad Complutense de Madrid, Madrid, Spain

development of some of the most promising inorganic nanocarriers, such as mesoporous silica nanoparticles, metal–organic nanoparticles and graphene nanosheets, as examples of materials with rigid, hybrid and soft nature, respectively, is presented. In addition, the role of electron microscopy in the nanoparticle characterization as well as in understanding the interactions with their biological targets is described.

## Inorganic nanocarriers for drug delivery applications

Inorganic nanoparticles, especially those with a porous nature, have emerged as powerful materials for drug delivery applications. One relevant characteristic of these materials is their high loading capacity, with external surface areas ranging from values between 500–10 000 m<sup>2</sup> g<sup>-1</sup>. Additionally, their pore network is easily tunable, which allows the transport of molecules with very different sizes, from macromolecules such as proteins, enzymes, DNA or RNA strands to small molecules such as antibiotics or cytotoxic compounds, among others. Both features allow the delivery of a high number of therapeutic species with very different natures, which is valuable for combination antitumoral therapy.<sup>10,11</sup> Besides these properties, inorganic carriers present other interesting characteristics such as low toxicity and immunogenicity, easy and cheap production, and high chemical and mechanical resistance, which make them excellent materials for clinical applications. However, due to the lack of flexibility, which is commonly exhibited by the majority of inorganic nanocarriers, their diffusion within living tissues is specially hampered. This fact compromises the nanocarrier distribution along the affected tissue and therefore diminishes the efficacy of the therapy. Despite this fact, the use of inorganic nanoparticles in medicine has been widely studied, and several strategies have been proposed in order to exploit their advantages while alleviating their limitations, as is described in this review.

### Mesoporous silica nanoparticles (MSNs)

There is a wide arsenal of synthetic methods for the production of MSNs with different morphologies such as spherical, rod, hollow or rattle, among others.<sup>12–15</sup> Particle morphology plays a key role in the cell internalization process. Therefore, its characterization by scanning electron microscopy (SEM)<sup>9</sup>—to monitor the surface fine structure and morphology—and transmission electron microscopy (TEM)<sup>8</sup>—to have access to the 3D morphology, the crystalline structure and the local chemical composition—is essential in order to get a proper insight of the biological properties of these systems.<sup>16,17</sup> Pore diameter is another important feature of MSNs. As in the previous case, there are many different synthetic methods which allow obtaining materials with pores from 2 nm, suitable for the delivery of small therapeutic agents (antibiotics, cytotoxic compounds, vitamins, *etc.*), to a few tens of nanometres, required for the transport of macromolecules such as proteins or nucleotide strands. Additionally, the pore distribution and order can also be controlled; thus, MSNs can be obtained with parallel,<sup>18</sup> radial,<sup>19</sup> fibrous<sup>20</sup> or dendritic

pore structures,<sup>21</sup> all of them being clearly observable by TEM. Recently, Yu *et al.* described the synthesis of beautiful MSNs with a core–cone pore structure, similar to the flower *Dahlia hortensis*, which presents narrowly packed curved petals surrounding a central core.<sup>22</sup> In this work, the authors employed electron tomography technique to describe the original morphology. Electron tomography records a series of images in which the orientation of the specimen is varied relative to the incident beam.<sup>23</sup> As a result, the image series contains all the information required to perfectly define the 3D structure of the novel structure. The study revealed that besides its beauty, this system had an astonishingly high pore volume of 2.59 cm<sup>3</sup> g<sup>-1</sup> and pore diameter of 45 nm, which also allowed the transport of big proteins (>100 kDa) in large numbers. The silica network can be also altered through substitution of Si atoms by other heteroatoms such as Al, Sn, Fe, Nb or Ti in order to modify the chemical nature of the material and, therefore, alter their catalytic or drug release properties.<sup>24</sup> The determination of the Si/heteroatom substitution grade and the exact location of the doping elements in the silica network can be analysed by spectroscopic techniques such as energy dispersive X-ray (EDX) and electron energy loss spectroscopy (EELS), associated to TEM operating in scanning mode (scanning TEM, STEM). In STEM mode, a small electron beam probe is focused and then rastered over the sample, while the inelastic processes, as the result of the interaction between the incident electron beam and the matter, allow the spatially resolved EELS or EDX elemental mapping for the identification and quantification of the elements present in the sample.<sup>8</sup> In 2010, Vallet-Regí and co-workers were pioneers in the detection of drug molecules confined within the pore network of MSNs.<sup>25</sup> In this work, pore channels were loaded with zoledronate, a drug widely employed in different bone pathologies. The material was studied by STEM microscope operating with a spherical aberration corrector in the probe (JEM-ARM200F) coupled with a high-energy resolution EELS spectrometer. The exceptional spatial resolution (0.08 nm) and the analytical capability of this instrumentation allowed the performance of spatially resolved analysis to detect the presence of the drug inside the pores. As shown in Fig. 1a, when the electron beam was perpendicularly oriented to the mesoporous channels, only Si and O were detected by EELS analysis, which was in accordance with the composition of silica walls. In opposition, if the electron beam was parallel to the channels (Fig. 1b), EELS analysis evidenced C and N located within the mesopores, which corresponds to the presence of zoledronate. This work proposed the first evidence that it could be possible to determine the presence of organic molecules within the pore network of inorganic materials by employing only electron microscopy.

In addition to loading the nanocarriers with therapeutic agents, smaller nanoparticles such as gold,<sup>26</sup> iron oxide,<sup>27</sup> silver nanocrystals,<sup>28</sup> and many others can be trapped within the mesoporous silica matrix. Thus, thanks to the presence of these metallic particles, photothermal properties, magnetic hyperthermia or antibacterial ability can be respectively added to enhance the potential clinical application of these devices. Metal particles

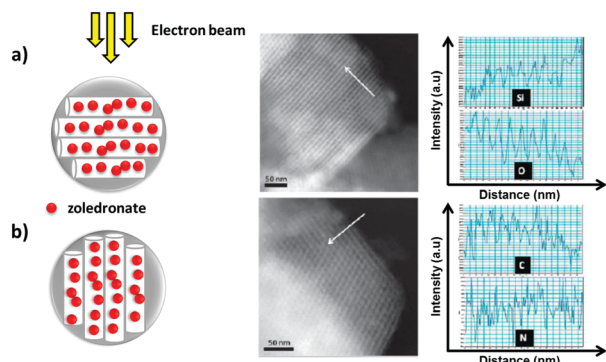


Fig. 1 Detection of drugs loaded within MSN channels by EELS with mesoporous channels: (a) perpendicular or (b) parallel to the electron beam. Si, O, C and N lines correspond to the intensity of the EELS Si-K; O-K; C-K and N-K edges, respectively.

coated with the mesoporous silica shell can be clearly observed by TEM imaging—in which image contrast is highly sensitive to the mass contrast—as well as by STEM using high-angle annular field imaging technique—in which image contrast is highly sensitive to the atomic number. In both, the different atomic numbers between the heavy metal atoms in comparison with the silica counterpart provides a clear difference in the contrast among both materials that permits perfect identification of the core-shell composite. Additionally, the particle composition can be analysed by EDX-STEM or EELS-STEM with high spatial resolution, and their degree of crystallinity can be further determined by high-resolution TEM analysis. Zink *et al.* have developed a hybrid dual-core MSN device which encapsulates in the same carrier superparamagnetic iron oxide nanoparticles (SPIONs) and  $\text{Yb}^{3+}/\text{Er}^{3+}$ -doped  $\text{NaYF}_4$  nanoparticles. This device allowed real-time monitoring of temperature in the particle's surroundings under alternative magnetic field exposure.<sup>29</sup> SPIONs generate heat once the magnetic field is applied, while  $\text{Yb}^{3+}/\text{Er}^{3+}$ -doped  $\text{NaYF}_4$  nanoparticles act as a nanothermometer because their luminescence is strongly dependent on the surrounding temperature. Therefore, by measuring the luminescence change when the magnetic field is applied, it is possible to determine the temperature surrounding the particle with high precision, which is of paramount importance in the development of magnetic field-responsive devices.<sup>30</sup> This device was characterized by combining high-resolution TEM, STEM and EDX mapping analysis, which showed that 70% of hybrid MSNs presented 1:1 ratio between SPIONs and  $\text{Yb}^{3+}/\text{Er}^{3+}$ -doped  $\text{NaYF}_4$  nanoparticles, with an average distance between them of around 8–9 nm, which indicated the excellent performance of the synthetic procedure. Unfortunately, the encapsulation of metallic particles within MSNs could result in a significant loading capacity reduction and, therefore, a limited therapeutic capacity in the case of drug delivery nanodevices. Recently, Li *et al.*<sup>31</sup> have developed Janus silver-MSNs, which combine the surface plasmon resonance (SPR) properties of silver with the excellent loading capacity of MSNs. Characterization by SEM, TEM and EDX mapping confirmed that this device presented a bullet-based Janus structure of approximately 300 nm, in which only one silver particle was embedded per silica rod.

In any case, the use of pure inorganic materials as drug carriers for clinical applications is very limited. The intravenous administration of naked inorganic particles usually leads to rapid elimination as a consequence of their capture by the mononuclear phagocyte system (MPS). MPS has evolved over millions of years in order to recognize foreign agents (such as these particles) and orchestrate their elimination.<sup>32</sup> The external surface of these drug carriers must be decorated with bio-organic moieties in order to avoid their premature capture. The most common strategy for enhancing their circulation time consists of the attachment of hydrophilic polymers such as polyethylene glycol (PEG)<sup>33</sup> or zwitterionic polymers.<sup>34</sup> The presence of these polymer chains on the nanocarrier surface hampers the adsorption of opsonins, which are proteins that trigger the MPS clearance pathway. Moreover, the attachment of hydrophilic polymers also enhances the colloidal stability of MSNs in biological fluids,<sup>35</sup> which is a very important parameter due to particle aggregation that not only reduces the circulation time within the blood stream but could also produce lethal embolism.<sup>36</sup> The introduction of PEG chains on the particle surface is difficult to confirm by electron microscopy techniques because these polymers are usually grafted in low amounts. Additionally, the sensitive nature of organic materials against electron beams further complicates the visualization by these techniques. For this reason, the grafting step was monitored using mass spectroscopic techniques such as nuclear magnetic resonance (NMR) or Fourier-transform infrared (FTIR).

Among the different types of MSNs, MCM-41 is one of the most widely employed types for clinical applications due to its unique pore structure. This pore network is characterized by the presence of parallel pores of 2–5 nm without interconnections between them. Once the nanocarrier is loaded with the therapeutic species, it is possible to block drug departure through the attachment of organic or inorganic moieties on the pore outlets, which act as caps. Therefore, stimuli-responsive materials can be easily synthesized by grafting these caps through reversible or cleavable bonds sensitive to adequate stimuli.<sup>37</sup> This stimuli-responsive property is especially important when the transported drug is toxic or can induce the appearance of severe side effects, as in the case of, for example, antitumoral compounds, some anti-inflammatory drugs or certain antibiotics. Nanocrystals such as SPIONs,<sup>38</sup> gold<sup>39</sup> or CdS,<sup>40</sup> among others, have been grafted on MSN surfaces through cleavable bonds in order to control the drug release behaviour (Fig. 2a). In these cases, the attached gatekeepers were clearly observable by TEM thanks to the presence of the heavy atoms (Fe, Au and Cd, respectively). However, if the employed gatekeepers do not present these heavy elements as is the case in the use of cyclodextrins,<sup>41</sup> DNA strands<sup>42</sup> or small molecules,<sup>43</sup> their detection by electron microscopy techniques is harder and requires the use spectroscopic techniques such as solid-state NMR or Fourier-transform infrared spectroscopy (FTIR), among others (Fig. 2b).

Other available strategies for controlling the drug departure process include coating the MSN surface with polymers able to experience either conformational changes in response to certain stimuli or be degraded in the presence of some conditions. Thus, thermosensitive polymers based on polyNIPAM have been

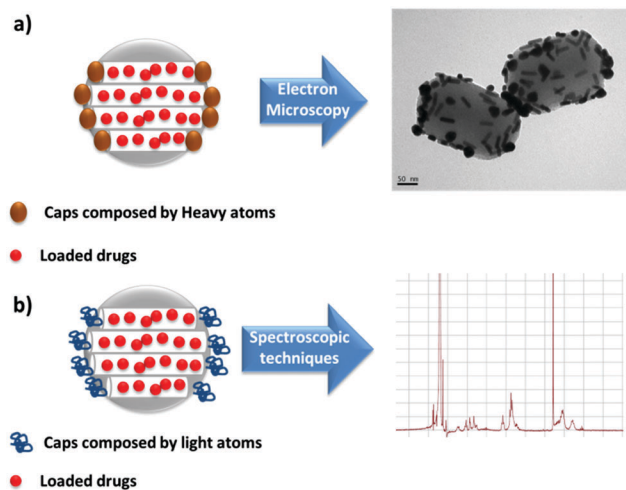


Fig. 2 Characterization techniques available for drug-loaded stimuli-responsive MSNs sealed with caps which present (a) heavy atoms and (b) light atoms (C, H, N and O).

widely employed in order to provide devices able to release their cargo once the temperature reaches a certain value.<sup>44</sup> When the temperature is maintained below the transition temperature, the polymer shell is completely hydrated and acts as a diffusion barrier that hampers the drug release, whereas if the temperature exceeds this value, the polymer suffers a collapse, thus allowing drug release. The thickness of the polymer layer is sufficiently wide (a few nanometres) to allow its visualization employing TEM. Interestingly, if the density of the polymer shells which envelop the MSN is low and the polymer chains are not cross-linked between them, the release behavior is just the opposite. In this case, the polymer layer, in its hydrated state, cannot prevent drug departure, but when the temperature reaches the transition temperature, some of the collapsed polymer chains block the pore outlet, preventing drug leakage.<sup>45</sup> In order to increase the image contrast between the silica and the polymer layer, different electro-opaque staining agents such as uranyl acetate or phosphotungstic acid can be employed. These agents present variable affinities with the organic layer, leading to highly or poorly contrasted micrographs, respectively. The same staining agents have also been employed to visualize other organic-based coatings for MSNs, such as lipid bilayers<sup>46</sup> or biopolymers,<sup>47</sup> among others. Other polymers have been produced in order to exploit different stimuli that trigger the drug release. Thus, polymers which contain functional groups sensitive to ultrasounds,<sup>48</sup> enzymes,<sup>49</sup> pH<sup>47</sup> or redox species<sup>50</sup> have been attached to the MSN surface in order to provide the capability to respond to these stimuli.

Despite the good performance exhibited by these devices in *in vitro* tests, the achievement of a perfect capping that completely avoids the premature release of the housed therapeutic agents is difficult, especially when they are exposed to a more complex environment such as the interior of a living system. An interesting alternative to the transport of active therapeutic agents is the use of prodrugs. Vallet-Regí *et al.* have developed a hybrid MSN able to generate *in situ* cytotoxic compounds once it is accumulated within tumoral cells.<sup>51</sup> The core of this device

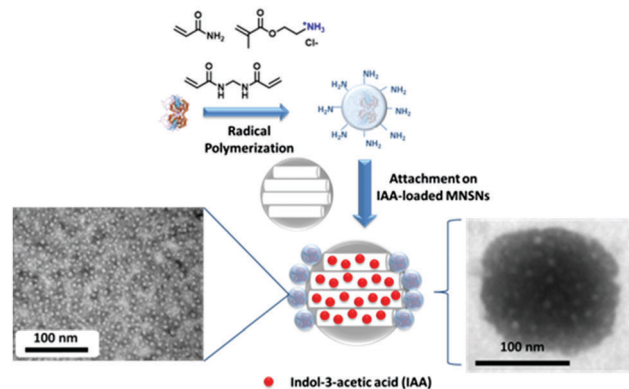


Fig. 3 MSNs coated with HRP nanocapsules. Left TEM image shows HRP nanocapsules alone, and right TEM image shows the complete system, both stained with phosphotungstic acid.

consists of amino-functionalized MSNs able to retain indol-3-acetic acid (IAA), a plant hormone completely harmless to humans. The enzyme responsible for the transformation of IAA into cytotoxic species, horseradish peroxidase (HRP), which is also innocuous, was firstly coated with a thin polymeric shell and then grafted on the MSN surface. This shell preserves its enzymatic activity and, at the same time, increases its resistance. These grafted enzyme nanocapsules were clearly observed by TEM with phosphotungstic acid as staining agent, which showed a homogeneous distribution over the entire particle surface (Fig. 3). This device was efficiently uptaken by different tumoral cells (neuroblastoma and leukaemia), and once inside, the sustained release of IAA followed by its transformation into cytotoxic species led to cell destruction.

### Metal-organic nanoparticles (MONs)

MONs are coordination polymers built using metal-ligand bonds and constitute another promising family of materials for drug delivery applications. Their potential is due to their particular properties such as: (i) high synthetic versatility regarding composition, shape, size, porosity and chemical properties, (ii) high loading capacity, (iii) biodegradability due to the labile metal bonds and (iv) the complementary properties provided by the presence of metal ions (magnetic, electronic or optical), which can be exploited for the production of theranostics devices thanks to the combination of their high capacity to transport and release therapeutic agents with imaging or diagnostic properties.

Two different categories can be differentiated within the MON family: nanoscale coordination polymers (NCPs), which present amorphous structure, and nanoscale metal-organic frameworks (NMOFs), which exhibit ordered porous structure.<sup>52</sup> The last group presents very high loading capacity as a consequence of the significant porosity of these materials. The loading capacity is lower in the first group, but in some cases, these carriers can encapsulate drugs up to 20% of their weight.<sup>53</sup> Additionally, NCPs can be synthesized as porous or hollow-based nanostructures in order to increase their cargo capacity.<sup>54</sup> As in the previous case, a review of the current state of the art of the use of MONs is not intended in this manuscript. Instead, our aim is only to present a few interesting examples of the application of this type of device in

nanomedicine while detailing the role of electron microscopy in their characterization. Some reviews which provide a broad panoramic view of the use of these devices for clinical applications can be found elsewhere.<sup>55,56</sup>

As has been commented above, NCPs present lower loading capacity than NMOFs, but the highly tuneable matrix composition allows the encapsulation of different therapeutic species. NCPs are usually formed by self-assembly process ruled by the nature of the metal and bridging ligands. The encapsulation process takes place during particle formation. The loading yield depends on the interactions between the cargo and the building blocks that form the particle. Thus, the control of these interactions has allowed different species such as fluorophores,<sup>53</sup> cytotoxic drugs<sup>57</sup> and also smaller nanoparticles such as SPIONs<sup>58</sup> to be effectively trapped within NCPs. Moreover, the bridging ligands themselves could be either therapeutic species or prodrugs, whose release during the degradation process may produce a sustained and significant increase in the loading capacity of those carriers.<sup>59</sup> As in the previous examples, the external surface of these carriers can be decorated with PEG<sup>60</sup> or lipid bilayers<sup>61</sup> in order to enhance their circulation time or to improve their uptake within the target cells. Electron microscopy provides important information about particle morphology and size distribution. The presence of heavy metal atoms within the particle structure is easily monitored by EDX, which could assess the homogeneous distribution of metal ions along the particle. Additionally, due to the fact that the trapped drugs are released as a consequence of the particle degradation, it is possible to test the drug release behaviour through observation by TEM and SEM of the particle erosion during the process.<sup>53</sup> NCPs can be designed to present stimuli-responsive drug release properties. As an example, one of the most employed stimuli is pH acidification, facilitated by the pH-sensitive nature of metal-ligand bonds. Che *et al.* have developed core-shell NCPs able to release different drugs (methotrexate, human glyoxalase I inhibitor or calcein) when the pH drops from physiological conditions (pH = 7.0) to the mild acidic conditions (pH = 5.0)<sup>62</sup> found within the endosomes, lysosomes and also in some tumoral tissues. Therefore, by exploiting this pH gradient, the encapsulated drugs can be released once the carriers have entered the target cells or reached the tumoral zone. The carrier is formed by a central core composed by the drugs coordinated with Fe<sup>2+</sup> or Zn<sup>2+</sup> cations and coated with a pH-degradable shell of bifunctional 1,4-bis(imidazol-1-ylmethyl)benzene (BIX) bridged by Zn<sup>2+</sup> atoms. Similar to previous examples, the core-shell structure of this device could be clearly observed by TEM imaging techniques due to the contrast difference between the core and the external shell, which also permits the exact measurement of the shell thickness. NCPs can exhibit interesting properties by themselves. Indeed, Zhang *et al.* synthesized coordination quantum dots (QD) employing Zn<sup>2+</sup> and potassium 3,4,9,10-perylenetetracarboxylate as building blocks, which proved to be a suitable material for labelling living cells.<sup>63</sup> The rounded shape morphology of these nanodevices with around 3 nm size was revealed by low-magnification TEM imaging, and the stabilization of the novel QD formed by the Zn-organic molecule

was confirmed by measuring their lattice parameters from high-resolution TEM images.

On the other hand, the highly regular pore network of NMOFs makes these materials ideal candidates for drug delivery applications. The pore diameter of MOFs can be engineered in order to house therapeutic agents such as anti-inflammatory,<sup>64</sup> antiarrhythmic<sup>65</sup> and antitumoral drugs,<sup>66</sup> to cite just a few examples. The ability to fine-tune the loading procedure requires a complete characterization of the pore network present in these materials. TEM appears again as an excellent tool to visualize the pore structure in individual particles, although, in this case, the damaging effect of the electron beam over the NMOFs needs to be considered. In general, the presence of covalent bonds and a composition involving light elements result in increased sensitivities to damage by electron beams. These two factors are common to many materials, but, in the case of NMOFs, porosity is an extra factor that can promote the loss of sample integrity because their organic linkers are prone to ionization, and the porous configuration tends to diminish its surface area and surface energy by collapsing the structure. Therefore, an extra effort is required to optimize the experimental TEM conditions for the characterization of these soft materials, generally based on the use of low acceleration voltages and low electron dose. Under these conditions, the morphology and crystallinity of the pore network have been characterized by diffraction and imaging TEM,<sup>67</sup> as well as by STEM<sup>68</sup> techniques, and even the location of encapsulated particles have been studied by electron tomography.<sup>69</sup>

As in precedent cases, in addition to drug encapsulation, it is also possible to trap other nanoparticles within the metal-organic matrix. Wöll *et al.* have recently reported the synthesis of hierarchically structured metal-organic framework multishells which contain magnetic nanocrystals in the particle core.<sup>70</sup> These devices, built by applying a layer-by-layer synthetic procedure, successively introduced multiple MOF shells with different compositions around a magnetic core. Each MOF shell provided a different property, resulting in nanodevices able to perform several tasks at the same time, such as multi-imaging and magnetic hyperthermia or stimuli-responsive drug release. Here, TEM characterization provided information about the particle thickness increase of each stage of MOF shell formation. In another related example, Duan *et al.* described the synthesis of other core-shell nanodevices composed by metallic cores coated with metal-organic framework shells.<sup>71</sup> This method was based on the previous growth of a polydopamine (PDA) layer around the central metallic nanoparticle. Then, metal-chelating activity provided by catechol groups present in dopamine directs and controls the growth of the MOF layer, affording the formation of discrete core-shell nanoparticles. The excellent adhesive capacity of PDA makes possible the application of this process to a vast number of nanoparticles with different chemical compositions, sizes and shapes. For example, this methodology allowed the construction of different MOF shells onto gold, mesoporous silica and polystyrene nanoparticles with spherical or star-shaped morphologies, thus providing a beautiful collection of hybrid nanodevices which combine different properties (Fig. 4).

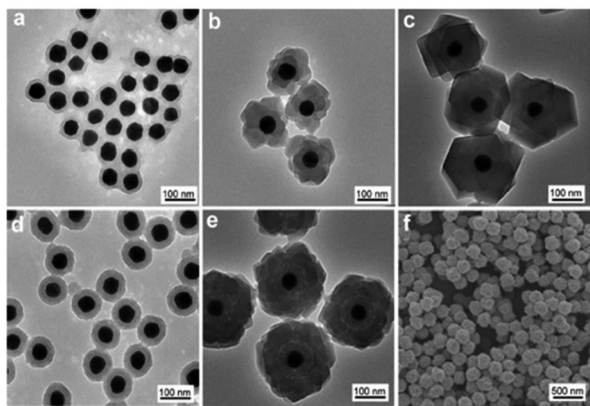


Fig. 4 (a–e) TEM images of Au nanoparticles coated with multishells of PDA and MOF (ZIF-8) of different thicknesses. (f) SEM image of Au nanoparticles coated with a multishell of PDA and MOF (ZIF-8). Extracted from ref. 71. Reprinted with permission from Zhou *et al.* (2015) Copyright © 2015, American Chemical Society.

As in the previous materials, EDX mapping provides information about the atomic composition of each layer.<sup>72</sup>

### Carbon nanoparticles

Carbon nanocarriers can be synthesized in the laboratory mainly in two different forms: carbon nanotubes (CNTs) and graphene oxide (GO) nanosheets. The observation of carbon-based materials by electron microscopy techniques has been traditionally limited by the sensitivity of light elements to electron irradiation. However, the successful implementation of aberration correctors into conventional TEM microscopes has contributed significantly to improving the spatial resolution and increasing the signal-to-noise ratio while operating at low voltages. These recent improvements offer an unprecedented opportunity to investigate carbon-based nanomaterials, reducing the damage by imaging at voltages of 60–80 kV or even lower.<sup>73</sup>

CNTs are molecular-scale tubes formed by graphene sheets rolled up into cylindrical hollow shapes with variable lengths, which can vary from hundreds of nanometres to microns. These materials can transport different therapeutic compounds, which are either adsorbed on the external surface or housed in the inner cavity. This cavity can present a diameter of 0.4–2 nm in the case of single-walled carbon nanotubes (SWCNTs) and 2–100 nm for multi-walled carbon nanotubes (MWCNTs). One of the first molecules encapsulated within the inner space of CNTs was another carbon allotrope, the Buckminster fullerene C<sub>60</sub>.<sup>74</sup> It was observed by high-resolution TEM operating at 100 kV, which provided nice images of self-assembled chains of fullerenes within CNTs, like beans inside a nanometric peapod. The spatial resolution achieved even before the implementation of aberration correctors allowed the accurate measurement of the intermolecular separation of each C<sub>60</sub> of around 1 nm. Other fullerenes, such as C<sub>70</sub> or Ce@C<sub>82</sub>, have been loaded within CNTs with different diameters in order to study the orientation and the capacity of these molecules to perform motions within the tubular structure.<sup>75</sup> Many other different molecules have also

been encapsulated within CNTs,<sup>76</sup> although the preferential loading location is the external surface, which can achieve up to 2500 m<sup>2</sup> g<sup>-1</sup>. Thus, antitumoral drugs such as doxorubicin<sup>77,78</sup> have been adsorbed or covalently grafted on the SWCNT surface in order to destroy malignant cells.

CNTs' aqueous solubility is really poor, and therefore, their application as drug carriers requires prior functionalization with polar groups or hydrophilic polymers. As in the already-discussed materials, these devices can be decorated with different moieties in order to provide useful properties which improve their performance as drug delivery systems.<sup>79</sup> Two interesting reported examples of CNTs as nanomedical platforms are the devices obtained by decoration of their surface with cationic functional groups, which permitted the delivery of DNA<sup>80</sup> or RNA<sup>81</sup> sequences into diseased cells, or the device functionalized with specific peptides able to induce strong immune responses on immune cells, which proved to be an immune activator in vaccination.<sup>82</sup> Additionally, different species can be loaded both in the inner cavity and in the external surface, like CNTs decorated with folate and loaded with doxorubicin and iron oxide nanoparticles.<sup>78</sup> The latter particles were formed *in situ* within the inner part of CNTs by encapsulation of Fe<sup>3+</sup> salts followed by reductive treatment. Observation by TEM confirmed the presence of the metallic nanoparticles of 5–7 nm diameter at the central cavity. These iron oxide particles enhanced the internalization of the carriers within tumoral areas by magnetic guidance. Similar to the case of MSNs, the ends of CNTs can be sealed with different moieties in a reversible way in order to control the release of a drug trapped within the inner section, producing a so-called nanobottle. Pastorin *et al.* have employed gold nanoparticles as pore caps in order to retain cis-platin within CNTs.<sup>83</sup> Gold nanocaps were functionalized with 1-octadecanethiol and absorbed by hydrophobic interactions on the nanotube tips as a consequence of their large interaction. The attachment of these caps significantly hampered the drug departure, achieving a more sustained drug release profile that improved the cytotoxic capacity of these devices against tumoral cells. The presence of cis-platin inside CNTs was detected by TEM, showing that high-contrast dots within CNTs could be confirmed as platin species by EDX analysis (Fig. 5).

Graphene is a 2D material formed by one or a few layers of sp<sup>2</sup>-hybridized carbon atoms covalently bound, forming a honeycomb framework. The atomic structure present in the carbon network exerts great influence on the final properties. As we mentioned above, aberration-corrected TEM<sup>84</sup> and STEM<sup>85</sup> are two powerful techniques to study the graphene framework with extraordinary precision. On the one hand, imaging techniques with atomic resolution provide essential information about the atomic configurations at graphene boundaries or the presence of single atom dopants,<sup>85,86</sup> on the other hand, their electronic properties can be locally explored by high-resolution STEM-EELS.<sup>87</sup> The combination of both imaging and spectroscopy techniques with atomic resolution permits the direct visualization and identification of changes in the electronic structure of the graphene—and therefore in its electro-optic properties—originated by presence of punctual defects or single-atom doping, thus

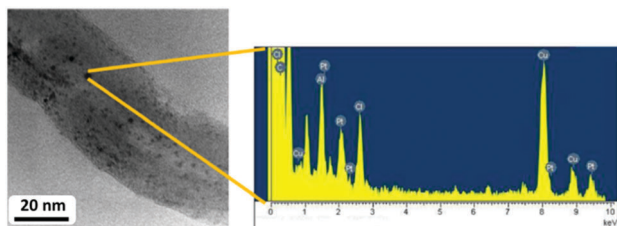


Fig. 5 TEM image of CNTs loaded with cis-platin, observable as dark dots, and EDX analysis, which confirms the presence of platinum. Extracted from ref. 83. Reprinted with permission from Li *et al.* (2012) Copyright © 2011 Elsevier Ltd. All rights reserved.

shedding light on fundamental scientific questions. Besides its excellent electric and thermal conductivity and its high mechanical strength, highly suitable for materials science, graphene also has really high external surface ( $2630 \text{ m}^2 \text{ g}^{-1}$ ), which makes it an excellent material for drug delivery applications. Nevertheless, due to the poor solubility of graphene in water, it should be oxidized to graphene oxide (GO) in order to increase its dispersability in biological fluids. For this reason, this oxidised form not only would have better colloidal stability in water but also would present oxygenated functional groups such as hydroxyls, epoxy and carboxylic acid, as recently probed by quantitative STEM-EELS.<sup>88</sup> The presence of these functional groups allows further attachment of different biological moieties for improving its performance. Oppositely to pure graphene, which retains drugs by  $\pi$ - $\pi$  stacking and hydrophobic interactions and therefore only efficiently retains highly hydrophobic drugs, GO is able to transport a wide number of therapeutic agents due to the presence of those hydrophilic groups on its surface.<sup>89</sup> Thus, different compounds have been transported by this type of carrier, such as antitumoral agents (doxorubicin<sup>90</sup> and topoisomerase I inhibitors<sup>91</sup>), imaging contrast agents,<sup>92</sup> magnetic nanocrystals<sup>93</sup> and gold nanoparticles,<sup>94</sup> among others. As in previously discussed nanocarriers, PEG has also been employed to modify the surface of GO in order to enhance its circulation time within the blood stream, showing negligible toxicity in mice models.<sup>95</sup>

GO nanosheets have been employed successfully as pore blockers in combination with porous inorganic nanocarriers. For example, Sailor *et al.* described the synthesis of a core-shell nanodevice formed by mesoporous silicon nanoparticles, with 10 nm-size pores capable of trapping small interfering RNA (siRNAs)<sup>96</sup> within their channels, which were further wrapped with GO nanosheets to slow down the release of the oligonucleotide strands.<sup>97</sup> Additionally, a specific targeting peptide derived from rabies virus glycoprotein was anchored on the GO surface in order to enhance the carrier selectivity for neural cells. TEM images confirmed that GO nanosheets were closely attached on the surface of porous silicon particles, which caused a significant reduction of the siRNA release rate. Graphene also presents a very interesting property for nanomedical applications with its capacity to generate heat under light irradiation, particularly near-infrared light, besides presenting high penetration capacity in living tissues.<sup>98</sup> Thus, the combination of the high loading capacity of GO together with the temperature

increase achieved under light irradiation has been used to improve the capacity to destroy tumoral cells with these nanodevices.<sup>99</sup> Ozin *et al.* described in detail the synthetic conditions required for the synthesis of a hybrid nanomaterial formed by graphene oxide and periodic mesoporous silica.<sup>100</sup> The characterization of this nanomaterial by STEM imaging revealed that the GO grid acted as template to guide the formation of a mesoporous silica layer, resulting in channels oriented vertically to the carbon plane. This hybrid composite combined the unique properties of graphene with the highly ordered pore network of mesoporous silica. This material has been employed for the treatment of malignant glioma, achieving good results in *in vitro* tests.<sup>101</sup> Thus, doxorubicin was loaded within the mesoporous silica channels, and a specific peptide sequence specific to the receptor chain 2 of interleukin 13 (overexpressed by glioblastoma cells) was anchored on the graphene surface. The combination of pH-triggered doxorubicin release when the nanodevice was uptaken by tumoral cells and its photothermal capacity when exposed to 808 nm laser beam produced a substantial increase in its cytotoxic capacity, converting this material into a promising candidate for the treatment of this unmet pathology.

## Observing the interaction with living systems

One of the main administration routes of nanomedicines is injection into the bloodstream. Therefore, one of the first living tissues that will contact with the carrier is blood, and this interaction mainly occurs with its cellular components: red blood cells, white blood cells and platelets. The interaction with these cells strongly depends on the composition, surface functionalization, morphology, size and aggregation state of the carrier. White blood cells are the principal components of the immune system and, therefore, would lead to particle clearance or triggering immune responses upon interaction with the carrier. Monocytes are cells responsible for the elimination of foreign bodies and usually capture circulating nanoparticles, especially when they are not conveniently functionalized. As mentioned above, particle surface decoration with PEG usually reduces the uptake by these cells as a direct consequence of the opsonin adsorption decrease. A nice example by Arruebo *et al.* studied the uptake of different inorganic nanocarriers by macrophages.<sup>102</sup>

Although TEM imaging techniques could be employed to image nanoparticles inside cells<sup>103</sup> because of the good spatial resolution achieved, the sample preparation requires many treatment processes, and some of them—such as centrifugation or cell fixation—can introduce modifications in the organelles, discouraging its use. Nevertheless, such preparation processes are not needed when using SEM, in which morphological/topological contrast and compositional information are separately obtained by selecting specific types of emitted electrons, known as secondary electrons (with energies smaller than 50 eV) and back-scattered electrons (with energies larger than 50 eV). Additionally, further compositional information is obtained through EDX analysis. One example of the capabilities of the SEM imaging

techniques is the use of secondary electron and backscattered electron imaging to observe nanocarriers on the cell membrane, where the semi-quantitative characterization of their atomic composition in the case of metal-containing particles was complemented by EDX.<sup>102</sup> The latest technical developments in SEM based on the use of field emission guns at low voltages allow the achievement of around 1 nm spatial resolution, which satisfies, in many cases, the spatial resolution requirements for the characterization of the nanoparticle–cell system.<sup>104</sup> In this sense, Havrdova *et al.* employed field-emission scanning electron microscopy and the application of gentle beam mode for observing in 3D with ultra-high resolution the nanoparticles' entry into mesenchymal cells, allowing visualization within endosomes (Fig. 6).<sup>105</sup> This technique was also employed for the observation of different types of inorganic nanoparticles (CeO<sub>2</sub>, TiO<sub>2</sub> and ZnO) with excellent performance.<sup>106</sup> The presence of heavy atoms allowed an accurate map of the nanoparticle distribution along the cell to be obtained. Another contribution to the topic by Hoogenboom *et al.* described the use of SEM fluorescence-integrated microscope for the visualization of particle endocytosis; this case combined the high resolution achieved with electron microscopy with the great versatility of fluorescent microscopy, which provided information about dynamic molecular processes inside the cell.<sup>107</sup>

Red blood cells (RBC) are the major cell component of blood, and therefore, to study the particle interaction with these cells is compulsory in order to properly evaluate the potential toxicity of each carrier. Trewyn *et al.* described the haemolytic activity of MSNs depending on their morphology, size and surface properties.<sup>108</sup> They studied these phenomena and found that small, round MSNs of 100 nm with MCM-41 structure barely disturbed the RBC membrane, while larger MSNs (600 nm) with SBA-15 structure provoked a strong disruption in the membrane and thus an enhanced particle internalization, which could cause haemolysis. Also, external functionalization played an important role in this process; it was observed that the higher functionalization grade results in lower interaction with the cell membrane. RBC can also be employed as model of non-phagocytic cells in order to study the potential toxicity of nanoparticles due to

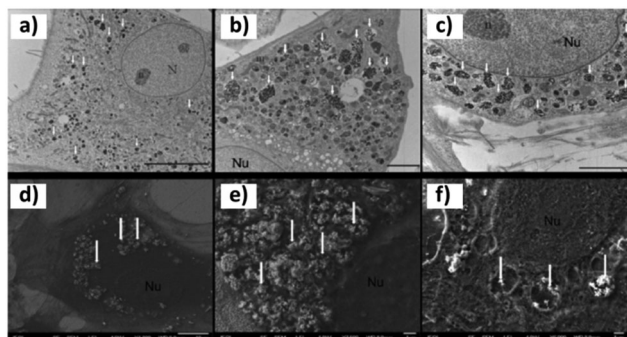


Fig. 6 Nanocarriers internalized within mesenchymal cells observed by TEM (a–c) and using field emission SEM (FE–SEM) (d–f). White arrows indicate the presence of nanoparticles within endosomes. Extracted from ref. 105. Reprinted with permission from Havrdova *et al.* (2014) Copyright © 2014 Elsevier Ltd.

the absence of phagocytic receptors on their surface or the actin–myosin system. Gehr *et al.* studied the internalization process of small gold nanoparticles with 25 nm diameter in RBC by employing electron microscopy techniques.<sup>109</sup> In this case, the internalization was easily monitored by conventional TEM due to the electron-dense character of gold atoms, which showed that the external surface charge did not play any role in the uptake process. Moreover, the particles crossed the membrane when they maintained their discrete nature, but they could not be uptaken when aggregated. Interestingly, TEM micrographs showed that these nanoparticles were never surrounded by membranes, which could mean that the nanosystems crossed the cell membrane by other mechanisms different from endocytosis, such as diffusion, transmembrane channels or “adhesive interactions.” TiO<sub>2</sub> nanoparticle internalization in the same cells was revealed by EELS by monitoring the titanium signal.

In the case of drug delivery carriers, the main goal is to enhance particle uptake in target cells while reducing as much as possible the internalization in healthy cells. This effect can be achieved by grafting targeting agents on the external surface of the nanocarriers. These targeting agents are molecules or biomacromolecules that interact or bind specific membrane receptors located mainly in the target cells. Thus, the presence of targeting groups provokes higher affinity between the nanocarrier and target cell membrane, thus favouring internalization, although particle uptake is a truly complex process which depends on each cell line. But in general, practically all nanoparticles access the inner cellular space by endocytosis.<sup>110</sup> Endocytosis is a complex energy-dependent process that introduces molecules or nanoparticles within the cell through an invagination process.<sup>111</sup> Once the particle makes contact with the membrane surface, the cell triggers the endocytic mechanism, which causes a membrane invagination that wraps the particle. Then, the particle enters the cytosolic space within a vesicle called endosome. These endosomes can transport the particles to different intracellular organelles, evolve to different structures such as lysosomes, which are in charge of the digestion of the uptaken moieties, or can be expelled again to the intracellular space in a process called transcytosis. There are different endocytic mechanisms, with receptor-mediated endocytosis being the most important one in the case of nanoparticle uptake.<sup>112</sup> In this mechanism, specific moieties which have been anchored on the particle surface recognize cell membrane receptors, enhancing the particle affinity by the target cell and promoting its internalization. Receptor-mediated endocytosis has been exhaustively employed in order to improve the selectivity of the nanocarrier against the tumoral cell, and correspondingly is the basis of targeted nanoparticles, as was mentioned above. Huang *et al.* studied in detail the influence that the shape of non-functionalized MSNs exerts in the endocytosis process into tumoral cells.<sup>16</sup> They synthesized three types of MSNs with different morphologies, one with spherical shape and two types of rod-shaped particles with different lengths. The internalization process of each particle was monitored by TEM, showing that in all cases, the particles were first internalized within a vesicle, which was merged with endosomes. Finally, the particle escaped from the endosome,

reaching the cytosolic space. Regarding their biological effect, the authors found that particles with lower aspect ratio (AR) produced lower interaction with the cells and, therefore, altered the cells' biological functions to a lower extent. Chan *et al.* studied the effect of size in the nanoparticle internalization process of gold and silver nanoparticles functionalized with antibodies.<sup>113</sup> The authors found that size played a critical role, not only in increasing or hindering particle uptake but also in the later location within the cell. The claimed reason was that the number of antibodies able to bind the cell receptors strongly depends on the number of receptors and, therefore, the particle size, being higher for larger particles. On other hand, the dissociation constant ( $K_d$ ) of antibody–receptor systems varies inversely with the size. Thus, smaller particles (2 nm) present similar  $K_d$  to free antibodies, whereas 40 nm particles have around 1000-fold lower  $K_d$ , which results in a stronger interaction with cell receptors. Another important parameter is the time required for wrapping the particle by the membrane. This time depends on the diffusion rate of cell receptors; this is a bottle-neck process for small or large nanoparticles. For this reason, internalization is optimal with medium-sized particles of 40–50 nm. One of the milestones in the characterization of biological systems is the possibility to observe them in their natural media. Cryo-electron microscopy, in which the biological sample is plunged into a cryogen in order to trap the sample in a thin film of vitreous ice, is one of the most employed techniques for the analysis of biological systems in a near-native, hydrated environment.<sup>114</sup> Although during the last five years, the technique has been increasingly experimented with as a result of the improvements in microscopes, imaging technologies, and computational approaches,<sup>115</sup> the process captures the biological–nanoparticle system at the moment of freezing, limiting its characterization. In this sense, many efforts have been devoted to the development of TEM instrumentation that allows observation in liquid media. Liquid cell electron microscopy<sup>116</sup> is a novel technique that allows the scientific community to apply the capabilities of the aberration-corrected electron microscopy to the imaging and analysis of liquid-based processes, like in the study of biological materials in liquid water. The measurement cell is usually prepared with two vacuum-tight electron-transparent membranes of silicon nitride that isolate the liquid from the vacuum while also confining it into a layer thin enough for imaging with transmitted electrons. One example of this technique is the recent study of 30 nm gold nanoparticle uptake by living cells.<sup>117</sup> This study employed a continuous flow of buffer solution through the measurement cell in order to maintain cell viability while the visualization was performed. The conventional electron microscopy nanoparticle uptake studies mentioned above usually require extensive conditioning, specimen sectioning treatment or harsh staining procedures that could generate difficult-to-distinguish electro-opaque clusters, thus making it difficult to obtain quantitative results free of artefacts. However, liquid cell electron microscopy acquires images from fully hydrated cells, which keep their functional structure, and therefore, it would be possible to obtain quantitative and accurate information about the three-dimensional distribution of the nanoparticles in the

entire cell, the total number of uptaken nanoparticles and the number of these particles located within vesicles.

## Conclusions and future prospects

The development of multifunctional nanocarriers able to specifically reach diseased cells without affecting healthy ones and, once there, to release their payload in response to an externally applied stimulus or as a consequence of the presence of certain internal stimuli characteristic to the pathological process has received huge attention, especially in the oncology field. One of the main reasons for the use of nanoparticles in oncology lies in their passive accumulation within solid tumours (EPR effect). However, this effect is not as universal as initially thought, but rather exhibits great heterogeneity depending on the tumour type, the patient and even the state of the therapy. Thus, the application of a nanocarrier-based therapy is not suitable for all types of cancer and should be carefully considered for each case. Additionally, the nanocarrier–biological interface environment should be studied in more detail. When a nanocarrier contacts with blood, it is immediately covered by a protein shell, which forms the so-called protein corona. This protein shell determines the particle fate because it forms the readable part of the nanodevice for cells. The corona formation is a dynamic process that suffers changes along the nanoparticle journey, and more knowledge about this process is required to control the selectivity and reproducibility of the nanotherapy. More research is needed in order to create nanomaterials able to overcome these barriers. With no doubt, electron microscopy, in particular TEM with spatial and analytical resolution at the atomic scale, is one of the essential tools required to gain knowledge needed for improving the efficacy of nanomedicines. Unfortunately, the resolution benefits of electron microscopy, both SEM and TEM, are associated with the challenge of preserving the functionalized nanocarriers as well as their biological environment during the experiments. The successful technological development of low-voltage microscopy with high resolution during recent years has critically improved the stability of the inorganic nanocarriers and the biological systems during their observation and local spectroscopic analysis, shedding light on still-unanswered scientific problems. Nevertheless, the future of electron microscopy in nanomedicine is necessarily linked to the complete development of the microscopy in the liquid state. The challenge of visualizing living systems in their native liquid state offers the possibility of obtaining high-resolution information while avoiding material damage from sample preparation, although a lot of work still has to be done on understanding the electron dose effects to evaluate which biological functions are preserved or missing during the TEM observation.

## Acknowledgements

This work was supported by the European Research Council (Advanced Grant VERDI; ERC-2015-AdG Proposal No. 694160)

and Spanish Government through the projects MAT2015-64831-R and MAT2014-58729-JIN.

## Notes and references

- 1 A. Ediriwickrema and W. M. Saltzman, *ACS Biomater. Sci. Eng.*, 2015, **1**, 64–78.
- 2 H. Chen, Z. Zhen, T. Todd, P. K. Chu and J. Xie, *Mater. Sci. Eng., R*, 2013, **74**, 35–69.
- 3 A. K. Mitra, V. Agrahari, A. Mandal, K. Cholkar, C. Natarajan, S. Shah, M. Joseph, H. M. Trinh, R. Vaishya, X. Yang, Y. Hao, V. Khurana and D. Pal, *J. Controlled Release*, 2015, **219**, 248–268.
- 4 M. W. Tibbitt, J. E. Dahlman and R. Langer, *J. Am. Chem. Soc.*, 2016, **138**, 704–717.
- 5 J. Mai, Y. Huang, C. Mu, G. Zhang, R. Xu, X. Guo, X. Xia, D. E. Volk, G. L. Lokesh, V. Thivyanathan, D. G. Gorenstein, X. Liu, M. Ferrari and H. Shen, *J. Controlled Release*, 2014, **187**, 22–29.
- 6 L. D. Field, J. B. Delehanty, Y. Chen and I. L. Medintz, *Acc. Chem. Res.*, 2015, **48**, 1380–1390.
- 7 S. Mura, J. Nicolas and P. Couvreur, *Nat. Mater.*, 2013, **12**, 991–1003.
- 8 *Aberration-Corrected Analytical Transmission Electron Microscopy*, ed. R. Brydson, John Wiley & Sons, Ltd, Chichester, UK, 2011.
- 9 M. Suga, S. Asahina, Y. Sakuda, H. Kazumori, H. Nishiyama, T. Nokuo, V. Alfredsson, T. Kjellman, S. M. Stevens, H. S. Cho, M. Cho, L. Han, S. Che, M. W. Anderson, F. Schüth, H. Deng, O. M. Yaghi, Z. Liu, H. Y. Jeong, A. Stein, K. Sakamoto, R. Ryoo and O. Terasaki, *Prog. Solid State Chem.*, 2014, **42**, 1–21.
- 10 L. Ma, M. Kohli and A. Smith, *ACS Nano*, 2013, **7**, 9518–9525.
- 11 R. R. Castillo, M. Colilla and M. Vallet-Regí, *Expert Opin. Drug Delivery*, 2017, **14**, 229–243.
- 12 M. Vallet-Regí, A. Rámila, R. P. del Real and J. Perez-Pariente, *Chem. Mater.*, 2001, **13**, 308–311.
- 13 M. Vallet-Regí, F. Balas and D. Arcos, *Angew. Chem., Int. Ed.*, 2007, **46**, 7548–7558.
- 14 S. Wu, X. Huang and X. Du, *J. Mater. Chem. B*, 2015, **3**, 1426–1432.
- 15 L. Li, Y. Guan, H. Liu, N. Hao, T. Liu, X. Meng, C. Fu, Y. Li, Q. Qu, Y. Zhang, S. Ji, L. Chen, D. Chen and F. Tang, *ACS Nano*, 2011, **5**, 7462–7470.
- 16 X. Huang, X. Teng, D. Chen, F. Tang and J. He, *Biomaterials*, 2010, **31**, 438–448.
- 17 T. Yu, A. Malugin and H. Ghandehari, *ACS Nano*, 2011, **5**, 5717–5728.
- 18 Y. Zhao, J. L. Vivero-Escoto, I. I. Slowing, B. G. Trewyn and V. S.-Y. Lin, *Expert Opin. Drug Delivery*, 2010, **7**, 1013–1029.
- 19 K. Möller, J. Kobler and T. Bein, *Adv. Funct. Mater.*, 2007, **17**, 605–612.
- 20 V. Polshettiwar, D. Cha, X. Zhang and J. M. Basset, *Angew. Chem., Int. Ed.*, 2010, **49**, 9652–9656.
- 21 D. Shen, J. Yang, X. Li, L. Zhou, R. Zhang, W. Li, L. Chen, R. Wang, F. Zhang and D. Zhao, *Nano Lett.*, 2014, **14**, 923–932.
- 22 C. Xu, M. Yu, O. Noonan, J. Zhang, H. Song, H. Zhang, C. Lei, Y. Niu, X. Huang, Y. Yang and C. Yu, *Small*, 2015, **11**, 5949–5955.
- 23 P. A. Midgley and R. E. Dunin-Borkowski, *Nat. Mater.*, 2009, **8**, 271–280.
- 24 J. Chen, F. Lu and J. Xu, *RSC Adv.*, 2015, **5**, 5068–5071.
- 25 M. Vallet-Regí, M. Manzano, J. M. Gonzalez-Calbet and E. Okunishi, *Chem. Commun.*, 2010, **46**, 2956–2958.
- 26 H. Li, L.-L. Tan, P. Jia, Q.-L. Li, Y.-L. Sun, J. Zhang, Y.-Q. Ning, J. Yu and Y.-W. Yang, *Chem. Sci.*, 2014, **5**, 2804–2808.
- 27 E. Ruiz-Hernández, A. Baeza and M. Vallet-Regí, *ACS Nano*, 2011, **5**, 1259–1266.
- 28 Y. Wang, X. Ding, Y. Chen, M. Guo, Y. Zhang, X. Guo and H. Gu, *Biomaterials*, 2016, **101**, 207–216.
- 29 J. Dong and J. I. Zink, *ACS Nano*, 2014, **8**, 5199–5207.
- 30 E. Guisasola, A. Baeza, M. Talelli, D. Arcos, M. Moros, J. M. D. La Fuente and M. Vallet-Regí, *Langmuir*, 2015, **31**, 12777–12782.
- 31 D. Shao, X. Zhang, W. Liu, F. Zhang, X. Zheng, P. Qiao, J. Li, W. Dong and L. Chen, *ACS Appl. Mater. Interfaces*, 2016, **8**, 4303–4308.
- 32 J. W. Nichols and Y. H. Bae, *Nano Today*, 2012, **7**, 606–618.
- 33 A. S. Karakoti, S. Das, S. Thevuthasan and S. Seal, *Angew. Chem., Int. Ed.*, 2011, **50**, 1980–1994.
- 34 J. T. Sun, Z. Q. Yu, C. Y. Hong and C. Y. Pan, *Macromol. Rapid Commun.*, 2012, **33**, 811–818.
- 35 Y. S. Lin, K. R. Hurley and C. L. Haynes, *J. Phys. Chem. Lett.*, 2012, **3**, 364–374.
- 36 S. P. Hudson, R. F. Padera, R. Langer and D. S. Kohane, *Biomaterials*, 2008, **29**, 4045–4055.
- 37 A. Baeza, M. Colilla and M. Vallet-Regí, *Expert Opin. Drug Delivery*, 2015, **12**, 319–337.
- 38 S. Giri, B. G. Trewyn, M. P. Stellmaker and V. S.-Y. Lin, *Angew. Chem., Int. Ed.*, 2005, **44**, 5038–5044.
- 39 F. Torney, B. G. Trewyn, V. S.-Y. Lin and K. Wang, *Nat. Nanotechnol.*, 2007, **2**, 295–300.
- 40 C.-Y. Lai, B. G. Trewyn, D. M. Jeftinija, K. Jeftinija, S. Xu, S. Jeftinija and V. S.-Y. Lin, *J. Am. Chem. Soc.*, 2003, **125**, 4451–4459.
- 41 J. Liu, Z. Luo, J. Zhang, T. Luo, J. Zhou, X. Zhao and K. Cai, *Biomaterials*, 2016, **83**, 51–65.
- 42 P. Zhang, F. Cheng, R. Zhou, J. Cao, J. Li, C. Burda, Q. Min and J. J. Zhu, *Angew. Chem., Int. Ed.*, 2014, **53**, 2371–2375.
- 43 D. He, X. He, K. Wang, J. Cao and Y. Zhao, *Langmuir*, 2012, **28**, 4003–4008.
- 44 A. de Sousa, D. A. Maria, R. G. de Sousa and E. M. B. de Sousa, *J. Mater. Sci.*, 2010, **45**, 1478–1486.
- 45 E. Guisasola, A. Baeza, M. Talelli, D. Arcos and M. Vallet-Regí, *RSC Adv.*, 2016, **6**, 42510–42516.
- 46 L. Wang, L. Wu, S. Lu, L. Chang, I. Teng, C. Yang and J. A. Ho, *ACS Nano*, 2010, **4**, 4371–4379.
- 47 M. Martínez-Carmona, D. Lozano, M. Colilla and M. Vallet-Regí, *RSC Adv.*, 2016, **6**, 50923–50932.
- 48 J. L. Paris, M. V. Cabañas, M. Manzano and M. Vallet-Regí, *ACS Nano*, 2015, **9**, 11023–11033.
- 49 A. Bernardos, L. Mondragón, E. Aznar, M. D. Marcos, R. Martínez-Mañez, F. Sancenón, J. Soto, J. M. Barat, E. Pérez-Payá, C. Guillem and P. Amorós, *ACS Nano*, 2010, **4**, 6353–6368.

- 50 Z. Luo, K. Cai, Y. Hu, L. Zhao, P. Liu, L. Duan and W. Yang, *Angew. Chem., Int. Ed.*, 2011, **50**, 640–643.
- 51 A. Baeza, E. Guisasola, A. Torres-Pardo, J. M. González-Calbet, G. J. Melen, M. Ramirez and M. Vallet-Regí, *Adv. Funct. Mater.*, 2014, **24**, 4625–4633.
- 52 C. He, D. Liu and W. Lin, *Chem. Rev.*, 2015, **115**, 11079–11108.
- 53 I. Imaz, M. Rubio-Martínez, L. García-Fernández, F. García, D. Ruiz-Molina, J. Hernando, V. Puentes and D. MasPOCH, *Chem. Commun.*, 2010, **46**, 4737–4739.
- 54 M. Hu, A. A. Belik, M. Imura and Y. Yamauchi, *J. Am. Chem. Soc.*, 2013, **135**, 384–391.
- 55 P. Horcajada, R. Gref, T. Baati, P. K. Allan, G. Maurin, P. Couvreur, G. Férey, R. E. Morris and C. Serre, *Chem. Rev.*, 2012, **112**, 1232–1268.
- 56 F. Novio, J. Simmchen, N. Vázquez-Mera, L. Amorín-Ferré and D. Ruiz-Molina, *Coord. Chem. Rev.*, 2013, **257**, 2839–2847.
- 57 F. Novio, J. Lorenzo, F. Nador, K. Wnuk and D. Ruiz-Molina, *Chem. – Eur. J.*, 2014, **20**, 15443–15450.
- 58 M. Borges, S. Yu, A. Laromaine, A. Roig, S. Suárez-García, J. Lorenzo, D. Ruiz-Molina and F. Novio, *RSC Adv.*, 2015, **5**, 86779–86783.
- 59 W. J. Rieter, K. M. Pott, K. M. L. Taylor and W. Lin, *J. Am. Chem. Soc.*, 2008, **130**, 11584–11585.
- 60 C. Poon, C. He, D. Liu, K. Lu and W. Lin, *J. Controlled Release*, 2015, **201**, 90–99.
- 61 R. C. Huxford, K. E. DeKrafft, W. S. Boyle, D. Liu and W. Lin, *Chem. Sci.*, 2012, **3**, 198–204.
- 62 L. Xing, Y. Cao and S. Che, *Chem. Commun.*, 2012, **48**, 5995–5997.
- 63 L. Zhang, X. Qian, L. Liu, Z. Shi, Y. Li, S. Wang, H. Liu and Y. Li, *Chem. Commun.*, 2012, **48**, 6166–6168.
- 64 Y. Yang, Q. Hu, Q. Zhang, K. Jiang, W. Lin, Y. Yang, Y. Cui and G. Qian, *Mol. Pharmaceutics*, 2016, **13**, 2782–2786.
- 65 J. An, S. J. Geib and N. L. Rosi, *J. Am. Chem. Soc.*, 2009, **131**, 8376–8377.
- 66 R. Anand, F. Borghi, F. Manoli, I. Manet, V. Agostoni, P. Reschiglian, R. Gref and S. Monti, *J. Phys. Chem. B*, 2014, **118**, 8532–8539.
- 67 S. Turner, O. I. Lebedev, F. Schröder, D. Esken, R. A. Fischer and G. Van Tendeloo, *Chem. Mater.*, 2008, **20**, 5622–5627.
- 68 Q.-L. Zhu, J. Li and Q. Xu, *J. Am. Chem. Soc.*, 2013, **135**, 10210–10213.
- 69 K. A. Mkhoyan, A. W. Contryman, J. Silcox, D. A. Stewart, G. Eda, C. Mattevi, S. Miller and M. Chhowalla, *Nano Lett.*, 2009, **9**, 1058–1063.
- 70 S. Schmitt, M. Silvestre, M. Tsotsalas, A. L. Winkler, A. Shahnas, S. Grosjean, F. Laye, H. Gliemann, J. Lahann, S. Bräse, M. Franzreb and C. Wöll, *ACS Nano*, 2015, **9**, 4219–4226.
- 71 J. Zhou, P. Wang, C. Wang, Y. T. Goh, Z. Fang, P. B. Messersmith and H. Duan, *ACS Nano*, 2015, **9**, 6951–6960.
- 72 K. Deng, Z. Hou, X. Li, C. Li, Y. Zhang, X. Deng, Z. Cheng and J. Lin, *Sci. Rep.*, 2015, **5**, 7851–7855.
- 73 K. Suenaga, Y. Sato, Z. Liu, H. Kataura, T. Okazaki, K. Kimoto, H. Sawada, T. Sasaki, K. Omoto, T. Tomita, T. Kaneyama and Y. Kondo, *Nat. Chem.*, 2009, **1**, 415–418.
- 74 B. W. Smith, M. Monthieux and D. E. Luzzi, *Nature*, 1998, **396**, 323–324.
- 75 A. N. Khlobystov, D. Britz and G. A. D. Briggs, *Acc. Chem. Res.*, 2005, **38**, 901–909.
- 76 M. Koshino, T. Tanaka, N. Solin, K. Suenaga, H. Isobe and E. Nakamura, *Science*, 2007, **316**, 853.
- 77 Z. Liu, X. Sun, N. Nakayama-Ratchford and H. Dai, *ACS Nano*, 2007, **1**, 50–56.
- 78 R. Li, R. Wu, L. Zhao, Z. Hu, S. Guo, X. Pan and H. Zou, *Carbon*, 2011, **49**, 1797–1805.
- 79 M. Prato, K. Kostarelos and A. Bianco, *Acc. Chem. Res.*, 2008, **41**, 60–68.
- 80 D. Pantarotto, R. Singh, D. McCarthy, M. Erhardt, J.-P. Briand, M. Prato, K. Kostarelos and A. Bianco, *Angew. Chem., Int. Ed.*, 2004, **43**, 5242–5246.
- 81 A. K. Varkouhi, S. Foillard, T. Lammers, R. M. Schiffelers, E. Doris, W. E. Hennink and G. Storm, *Int. J. Pharm.*, 2011, **416**, 419–425.
- 82 D. Pantarotto, C. D. Partidos, J. Hoebeke, F. Brown, E. Kramer, J.-P. Briand, S. Muller, M. Prato and A. Bianco, *Chem. Biol.*, 2003, **10**, 961–966.
- 83 J. Li, S. Q. Yap, S. L. Yoong, T. R. Nayak, G. W. Chandra, W. H. Ang, T. Panczyk, S. Ramaprabhu, S. K. Vashist, F. S. Sheu, A. Tan and G. Pastorin, *Carbon*, 2012, **50**, 1625–1634.
- 84 A. W. Robertson and J. H. Warner, *Nanoscale*, 2013, **5**, 4079–4093.
- 85 P. Y. Huang, C. S. Ruiz-Vargas, A. M. van der Zande, W. S. Whitney, M. P. Levendorf, J. W. Kevek, S. Garg, J. S. Alden, C. J. Hustedt, Y. Zhu, J. Park, P. L. McEuen and D. A. Muller, *Nature*, 2011, **469**, 389–392.
- 86 O. L. Krivanek, M. F. Chisholm, V. Nicolosi, T. J. Pennycook, G. J. Corbin, N. Dellby, M. F. Murfitt, C. S. Own, Z. S. Szilagyi, M. P. Oxley, S. T. Pantelides and S. J. Pennycook, *Nature*, 2010, **464**, 571–574.
- 87 K. Suenaga and M. Koshino, *Nature*, 2010, **468**, 1088–1090.
- 88 A. Tararan, A. Zobelli, A. M. Benito, W. K. Maser and O. Stéphan, *Chem. Mater.*, 2016, **28**, 3741–3748.
- 89 K. A. Mkhoyan, A. W. Contryman, J. Silcox, D. A. Stewart, G. Eda, C. Mattevi, S. Miller and M. Chhowalla, *Nano Lett.*, 2009, **9**, 1058–1063.
- 90 X. Sun, Z. Liu, K. Welsher, J. T. Robinson, A. Goodwin, S. Zaric and H. Dai, *Nano Res.*, 2008, **1**, 203–212.
- 91 Z. Liu, J. T. Robinson, X. Sun and H. Dai, *J. Am. Chem. Soc.*, 2008, **130**, 10876–10877.
- 92 W. Miao, G. Shim, G. Kim, S. Lee, H. J. Lee, Y. B. Kim, Y. Byun and Y. K. Oh, *J. Controlled Release*, 2015, **211**, 28–36.
- 93 S. Moradi, O. Akhavan, A. Tayyebi, R. Rahighi, M. Mohammadzadeh and H. R. Saligheh Rad, *RSC Adv.*, 2015, **5**, 47529–47537.
- 94 S. Gao, L. Zhang, G. Wang, K. Yang, M. Chen, R. Tian, Q. Ma and L. Zhu, *Biomaterials*, 2016, **79**, 36–45.
- 95 K. Yang, J. Wan, S. Zhang, Y. Zhang, S. T. Lee and Z. Liu, *ACS Nano*, 2011, **5**, 516–522.
- 96 D. Moazed, *Nature*, 2009, **457**, 413–420.
- 97 J. Joo, E. J. Kwon, J. Kang, M. Skalak, E. J. Anglin, A. P. Mann, E. Ruoslahti, S. N. Bhatia and M. J. Sailor, *Nanoscale Horiz.*, 2016, **1**, 407–414.

- 98 J. T. Robinson, S. M. Tabakman, Y. Liang, H. Wang, H. Sanchez Casalongue, D. Vinh and H. Dai, *J. Am. Chem. Soc.*, 2011, **133**, 6825–6831.
- 99 G. Gonçalves, M. Vila, M. T. Portolés, M. Vallet-Regi, J. Gracio and P. A. A. P. Marques, *Adv. Healthcare Mater.*, 2013, **2**, 1072–1090.
- 100 Z.-M. Wang, W. Wang, N. Coombs, N. Soheilnia and G. A. Ozin, *ACS Nano*, 2010, **4**, 7437–7450.
- 101 Y. Wang, K. Wang, J. Zhao, X. Liu, J. Bu, X. Yan and R. Huang, *J. Am. Chem. Soc.*, 2013, **135**, 4799–4804.
- 102 B. Díaz, C. Sánchez-Espinel, M. Arruebo, J. Faro, E. De Miguel, S. Magadán, C. Yagüe, R. Fernández-Pacheco, M. R. Ibarra, J. Santamaría and Á. González-Fernández, *Small*, 2008, **4**, 2025–2034.
- 103 A. K. Gupta and M. Gupta, *Biomaterials*, 2005, **26**, 3995–4021.
- 104 S. Asahina, T. Togashi, O. Terasaki, S. Takami, T. Adschiri, M. Shibata and N. Erdman, *Microsc. Anal.*, 2012, **26**, S12–S14.
- 105 M. Havrdova, K. Polakova, J. Skopalik, M. Vujtek, A. Mokdad, M. Homolkova, J. Tucek, J. Nebesarova and R. Zboril, *Micron*, 2014, **67**, 149–154.
- 106 G. Plascencia-Villa, C. R. Starr, L. S. Armstrong, A. Ponce and M. José-Yacamán, *Integr. Biol.*, 2012, **4**, 1358–1366.
- 107 N. Liv, D. S. B. van Oosten Slingeland, J.-P. Baudoin, P. Kruit, D. W. Piston and J. P. Hoogenboom, *ACS Nano*, 2016, **10**, 265–273.
- 108 Y. Zhao, X. Sun, G. Zhang, B. G. Trewyn, I. I. Slowing and V. S.-Y. Lin, *ACS Nano*, 2011, **5**, 1366–1375.
- 109 B. M. Rothen-Rutishauser, S. Schürch, B. Haenni, N. Kapp and P. Gehr, *Environ. Sci. Technol.*, 2006, **40**, 4353–4359.
- 110 T. G. Iversen, T. Skotland and K. Sandvig, *Nano Today*, 2011, **6**, 176–185.
- 111 G. Sahay, D. Y. Alakhova and A. V. Kabanov, *J. Controlled Release*, 2010, **145**, 182–195.
- 112 H. M. Ding and Y. Q. Ma, *Biomaterials*, 2012, **33**, 5798–5802.
- 113 W. Jiang, B. Y. S. Kim, J. T. Rutka and W. C. W. Chan, *Nat. Nanotechnol.*, 2008, **3**, 145–150.
- 114 E. Callaway, *Nature*, 2015, **525**, 172–174.
- 115 E. Binshtein and M. D. Ohi, *Biochemistry*, 2015, **54**, 3133–3141.
- 116 F. M. Ross, *Science*, 2015, **350**, 1490.
- 117 D. B. Peckys and N. de Jonge, *Nano Lett.*, 2011, **11**, 1733–1738.